Glass- and crystal-forming model based on a granular two-dimensional system

A. Escobar, C. Tapia-Ignacio, and F. Donado[*]
Instituto de Ciencias Básicas e Ingeniería de la Universidad Autónoma del Estado de Hidalgo-AAMF, Pachuca 42184, Pachuca, México

J. L. Arauz-Lara[†]
Instituto de Física "Manuel Sandoval Vallarta," Universidad Autónoma de San Luis Potosí, Alvaro Obregón 64, 78000 San Luis Potosí, S.L.P., México

R. E. Moctezuma[‡]
CONACYT-Instituto de Física "Manuel Sandoval Vallarta," Universidad Autónoma de San Luis Potosí, Alvaro Obregón 64, 78000 San Luis Potosí, S.L.P., México

(Received 2 May 2019; revised manuscript received 26 March 2020; accepted 6 May 2020; published 29 May 2020; corrected 5 June 2020)

We study a two-dimensional system of magnetic particles under an alternating magnetic field. The particles are settled on the surface of a negative lens where they tend to sediment toward the center due to gravity. The effective temperature is controlled by the intensity of the applied magnetic field. The system is cooled down from a gaslike state to a solidlike state at different rates. We observe that for some slow cooling rates the final configuration of system is a hexagonal compact arrange, while for the faster cooling rates the final configurations are glasslike states. We followed the time evolution of the system, which allows us to determine in detail changes in quantities such as the interparticle distance. We determine the glass transition temperature for different cooling rates, finding that such temperature increases as the cooling rate decreases, in contrast with some other glass-forming liquids.

DOI: 10.1103/PhysRevE.101.052907

I. INTRODUCTION

The understanding of nonequilibrium processes, such as the slowing down of structural relaxations in a system when it is approaching the solid state from the liquid side as it is cooling down, has been of interest for several decades [1–4]. A direct microscopic description face complex and challenging technological problems, for instance, tracking many particles in a fluid while it is cooling down, is not yet possible. The time resolution and the capacity of tracking each particle involves high technology not yet developed. Nevertheless, recent advances using interferometric techniques have shown that it is possible to track a single colloidal particle in a confined system [5–7]. Of course, the observation of the behavior of many particles inside a system is still a challenge. In order to shed light on the microscopic description of the phenomena appearing near a solidification transition, different macroscopic systems have been used as models for this process.

Experiments and computer simulations have shown that a good system for studying those phenomena is a colloidal suspension of magnetic particles. Such a system, exhibits spatially heterogeneous dynamics and an amorphous structure such as that observed in a glass-forming liquid [8–12]. On the other hand, another useful macroscopic model is a vibrating granular 2D system, where horizontal particle motions are slow enough to be tracked with a time resolution to resolve the ballistic regime [13]. Systems such as colloid-polymer mixtures, sticky particles, emulsions, foams, among other macroscopic systems have been used for the same purpose [3,4,14–17]. Those systems exhibit glasslike, liquidlike, and solidlike features when a physical quantity such as volume fraction, viscosity, polymer concentration, etc., is varied. In some systems, particle concentration plays the role of the inverse of the temperature; as particle concentration increases, the dynamics of the system slows down.

Macroscopic systems composed of small magnetic balls have been used as models for glass transition and crystallization studies. In these systems, energy input comes from mechanical vibrations, usually vertically, of the container. Cyclically sheared steel spheres have also been used to study the transition from glassy state to crystalline state [18–22]. In those systems, some aspects about the initial formation of crystalline nucleus was observed. In Ref. [23] crystallization was studied using a vibrating granular system placed on a slightly tilted surface. In that system, the inverse of the particle concentration takes the role of temperature.

In recent works, we studied a macroscopic model for fluid systems consisting of small magnetic balls settled on a plane and subjected to an alternating magnetic field perpendicular to the plane of motion. This mechanism to supply energy does not require the system to vibrate vertically as in other granular systems. Although the system is highly dissipative, it reaches

[*]Corresponding author: fernando@uaeh.edu.mx
[†]arauz@ifisica.uaslp.mx
[‡]rosario@ifisica.uaslp.mx

a stationary state. According to the Ornstein-Uhlenbeck process theory, the resulting motion has all the characteristics of Brownian motion, as we have shown in Ref. [24]. We have also shown that the particle velocity distribution is a Maxwell-Boltzmann distribution, and the effective temperature is proportional to the amplitude of the magnetic field [25]. We also found that a sudden quenching conducts the system from a liquidlike behavior to a solidlike behavior where aging can even be observed [24–26]. In those experiments, the system was spatially homogeneous, so it remains in the fluid phase structure. In contrast, in others systems, crystallization is a problem that needs to be solved, for instance, by introducing a small percentage of polydispersity, either in size or in shape.

In the present work, we study solidification process leading to either crystalline or amorphous structures. Here we use a modification of the experimental setup that we have already reported on Refs. [24–28]. We changed the geometry of the surface from a plane to a curved surface. This system resembles the case of a Brownian particle trapped in a harmonic potential such as an optical tweezer [5–7]. In our case, we have many particles instead of a single particle, and we are able to track the trajectories of all of them. By varying the magnetic field, the effective temperature is modulated. The system is almost an ideal 2D system since the particles are always in contact with the curved surface.

We provide a characterization of the structural properties of this system using the same analysis as in the flat surface case, namely, the distribution of the Voronoi polygon areas [27]. In the system studied before, with the flat surface, we used this tool to characterize the structural properties at different particle concentration [27]. In the present work, we use such methodology to characterize the structure of the system as it is cooled down.

II. EXPERIMENTAL SETUP

The particles in our system are settled on the glass surface of a lens of 50.8 mm in diameter and 250 mm of focus length. The particles are steel balls of 1 mm of diameter, ANSI 420 grade 1000 by Gimex S.A. The lens is located horizontally in the center of a Helmholtz coils arrangement which produces a vertical magnetic field, Fig. 1.

The coils are fed by a Kepco BOP 36-6 M power amplifier. This system of magnetic spheres is subjected to a sinusoidal magnetic field whose amplitude is gradually reduced at specific steps, ΔB_0, every second. The decreasing rate of the magnetic field amplitude is programed using the National Instruments LabView software and a DAQ card. The frequency was fixed at 9.24 Hz. Since the magnetic field plays the role of the temperature and, henceforth, we will refer to the amplitude of the magnetic field as the effective temperature [25]. In this sense, we model a cooling rate by gradually decreasing the amplitude of the magnetic field.

The dynamics of the system is explained as follows. The magnetic field induces a magnetic moment in each particle. As the field is changing its direction (up and down), particle's magnetic moment tends to change its direction to follow the direction of the field and minimize its potential energy. When the particle's magnetic moment points opposite to the field direction, it is in a very unstable state, and then it rotates in a random direction to align with the magnetic field. In the process of following the magnetic field direction, the particles rotate and roll, experiencing repulsive contact forces due to the other particles that tend to separate them. Additionally, due to the curvature of the surface, the particles experiment the effect of the gravity that forces them to move toward the center of the lens. Thus, the motion is more complex than on a plane and depends not only on frequency and amplitude of the magnetic field but also on the position of the particle respect to the center of the lens. In this system, it is common to observe random motion combined with circular motion around the center of the lens.

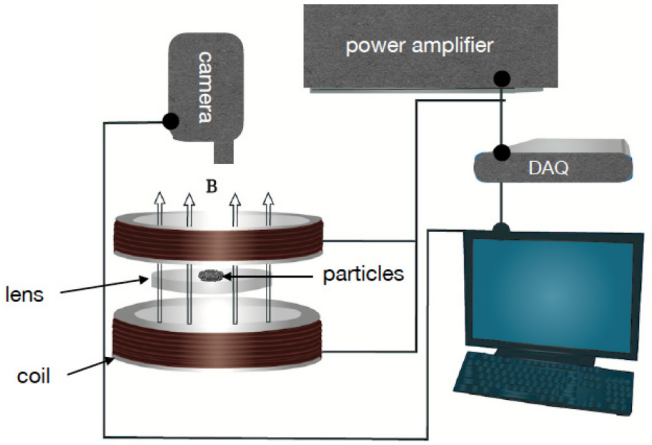

FIG. 1. Experimental setup. The coils in a Helmholtz arrangement produces a vertical magnetic field. The decreasing rate is controlled by a data acquisition card.

A HandyCam was used to record the dynamics of the system. We obtained runs of 5 min of video in a standard resolution of 480×640 pixels at 30 fps in AVI interlaced format. At this capture rate, the particle positions were not always well defined, and thus we use a filter to deinterlace the video frames to obtain well-defined image sequences with a resolution of $\tau = 1/60$ s.

Since the surface of the lens is curved, the real position of the particle with respect to the axis of symmetry is different from that observed with the camera from above; however, this difference is negligible. For our system, with the focal distance 250 mm and a lens diameter 50.8 mm, the maximum error at 25 mm from the axis is 0.17%. The particle acquires its maximum kinetic energy when it passes through the center of the lens. As it moves away from the center, its kinetic energy is transformed into gravitational energy. If a particle reaches the edge of the lens, then its height is about 1.2 mm, which shows that the energy of a particle at this position is low.

III. EXPERIMENTAL RESULTS

The starting state of the system is a gaslike state. Then, a cooling process is carried out diminishing the amplitude of the magnetic field in steps with different amplitude. We carried out experiments at cooling rates $\Delta B_0 = 2, 1.4, 1, 0.6, 0.2, 0.14, 0.1, 0.06, 0.02$ G/s. We track every trajectory in the system for time intervals of 2.50 s. We

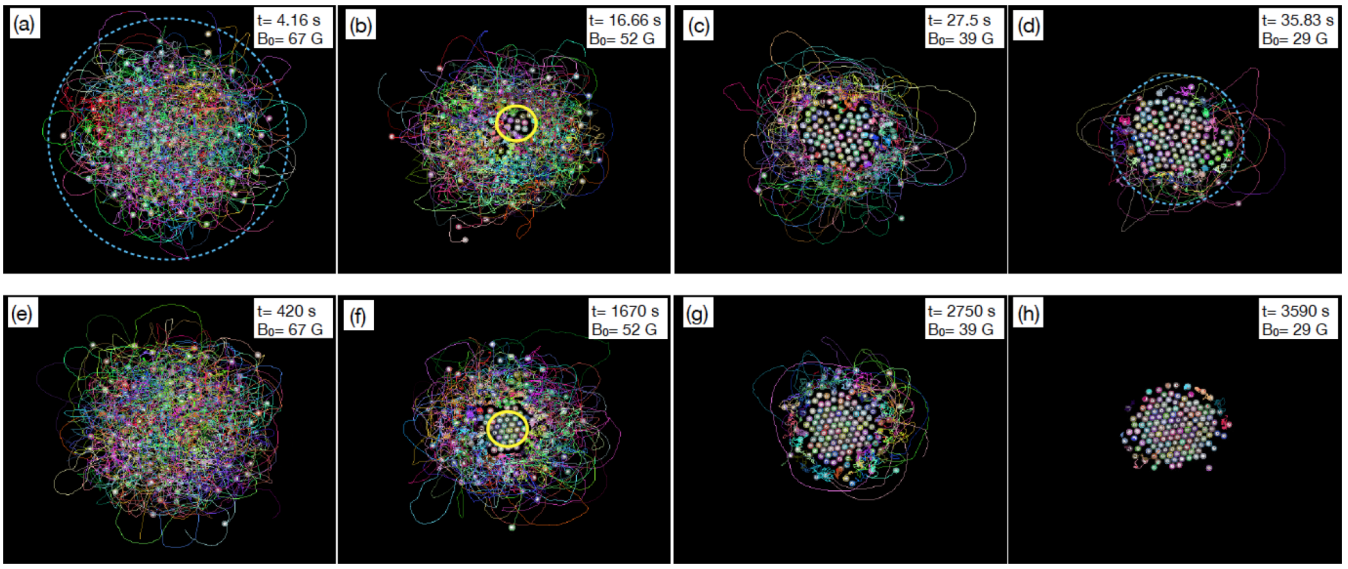

FIG. 2. Particle's trajectories. Top: Fast cooling rate 2 G/s. The circles in (b) and (f) shows the formation of a nucleus. Bottom: Slow cooling rate 0.02 G/s. As it can be seen here, for fast cooling the final configuration of the beads resembles a glass structure, while for slow cooling it exhibits a crystalline structure. The circles in (a) and (d) represent the area of configuration.

observe that the area occupied by the trajectories on the lens is a function of the magnetic field intensity. As temperature goes down, the system shrinks, driving the particles to a final configuration with a smaller area. Depending on the cooling rate, we observe a different temporal evolution of the configuration of the system [29].

Figure 2 shows two series of photos depicting the temporal evolution of the configurations corresponding to two different cooling rates. Each picture contains a superposition of all the trajectories (lines) in a time window; colors are for different trajectories. To obtain trajectories, the image sequences were binarized and then analyzed using the software ImageJ and its plugin Mosaic. At high temperatures, the trajectories covers much of the observation area. The pictures at the top, Figs. 2(a)–2(d), show the system at four different temperatures when the system is quickly cooled down ($\Delta B_0 = 2$ G/s), to very low effective temperature (near zero magnetic field). From these figures, we observe that the area occupied by the particles decreases quickly with temperature, which causes the particles to settle in a disordered configuration resembling a glass. In the pictures at the bottom, Figs. 2(e)–2(h), we present the evolution of the trajectories at the slowest cooling rate studied here, $\Delta B_0 = 0.02$ G/s. As it can be seen from these pictures, for this cooling rate the final configuration is crystalline. The lowest cooling rate we used corresponds to the threshold value below which the system always crystallizes.

As established in the nucleation theory, there is an energy barrier that must be overcome to produce nucleation. As the system is cooled down, the formation of a nucleus which leads the system to a solid phase is observed. The circles in Figs. 2(b) and 2(f) show the nucleus formed at a fast and at a slow cooling rate respectively. The value of the temperature indicated in these figures is the energy barrier that was overcome to produce nucleation.

We observe that the nucleus appears earlier for fast cooling rates than for the slow ones. The nucleus in Fig. 2(f) is more ordered than the nucleus in Fig. 2(b). During the formation of the nucleus in Fig. 2(f), it is observed that, first, a disordered aggregate is formed which eventually goes to an ordered configuration by the interaction with its neighbors. Thus, our system provide evidence that supports a two-step nucleation theory.

Typical final configurations and their respective fast Fourier transform (FFT) are shown in Fig. 3 for different cooling rates. In this figure we can observe that when the cooling is fast the final configuration is disordered, i.e., its corresponding FFT is typical of a glass configuration, Fig. 3(a). When the cooling is very slow the system forms a hexagonal closed packed array, Fig. 3(c). In latter case, the FFT image shows the typical arrangement of peaks in an ordered configuration, i.e., the hexagonal compact arrangement. The configuration formed by an intermediate cooling rate, Fig. 3(b), is not globally ordered but presents small regions where the particles form hexagonal closed packed structures. This corresponds to a polycrystalline arrangement and the FFT shows rings with inhomogeneities.

The particles spend more time near the center of the lens due to the gravitational force. This effect was quantified averaging the value of the intensities of pixels as a function of the radial distance. Here the average intensity value is proportional to the average density of particles in a region. The maximum intensity, at a distance r from the center, is obtained when the particles remain in this position throughout an entire study window. If the particles rarely visit a region, then it will appear with a very low intensity. Figure 4 shows the intensity profile of the final particle configuration at different effective temperatures for the fastest and the slowest cooling rate. From the figure it is seen that the particle density is higher for the slowest cooling, and it presents less fluctuations than for the fastest cooling rate. In both cases, we observe that at high temperatures the boundaries are diffuse, and as the temperature decreases, the boundaries are better defined.

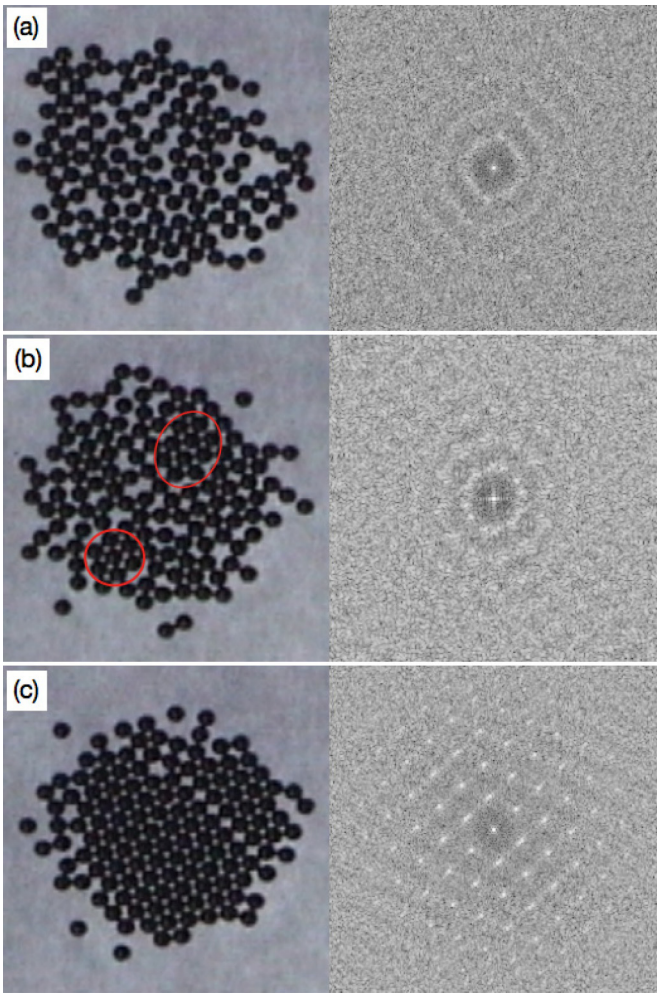

FIG. 3. Fast Fourier transform for three different final configurations. The cooling rate is higher in (a) and lower in (c). In (b) hexagonal closed packed structures, shown in circles, are locally formed.

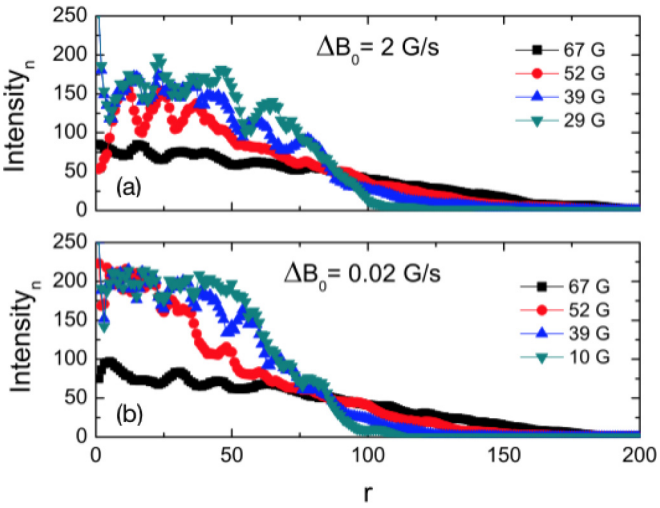

FIG. 4. Average intensity profile for the final configuration at (a) $\Delta B_0 = 2$ G/s and (b) $\Delta B_0 = 0.02$ G/s. This quantity is proportional to the average particle density at a distance r from the center of the lens. Here the particle density decreases with distance, showing that they move mostly near the center of the lens.

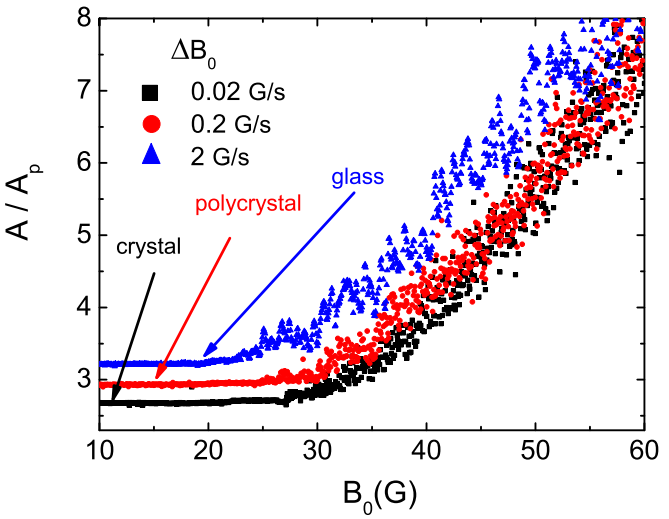

FIG. 5. Phase diagram: Normalized area (A/A_p) occupied by different configurations as the temperature is decreased at three different cooling rates. $A_p = 106.16$ mm^2 is the sum of the area of each particle. The area of the hexagons formed in close packing configuration is 116.8 mm^2.

Figure 5 depicts the behavior of the area occupied by the different configurations of the beads as a function of the temperature for three different cooling rates. To determine this area, first, we determined the positions of each particle. Then we obtain the variance around a centroid in x and y. The square root of the variance multiplied by two gives us the radius of the area that includes most of the particles in the distribution. The accuracy of the particle center detection was deduced to be 8% of a diameter (0.96 of a pixel), which was estimated using the width of the first peak of the pair correlation function [18]. The blue dotted circles in Figs. 2(a) and 2(d) show two examples of the area determined as described here. If we go through the graph in Fig. 5, from right to left, then two regions can be observed: one where the occupied area decreases fast as the temperature is lowered and another where it decreases slowly. This area is normalized with the total area of the beads (A_p). The inset in Fig. 6 shows linear fitting to the fast and slow regimes. These kind of curves are also observed in real liquids that are cooled at different rates [1]. Thus, following this similarity, we determine the corresponding so-called solid transition temperature, B_{0g}. Here B_{0g} was taken as the value where the linear functions intercept.

We observed a continuous transition from a glassy state at high cooling rate to a crystal state at slow cooling rate. For intermediate cooling rates, we observe the formation of different glassy states and the coexistence of crystal and glassy patches. The lowest cooling rate we used corresponds to the threshold value below which the system always crystallizes and, therefore, the glass transition temperature, B_{0g}, was only estimated for the cooling rates above $B_0 = 0.02$. Comparing the behavior of B_{0g}, in Fig. 6, with the behavior in different real glass-forming systems, it is observed an important difference; in our system, the glass transition temperature corresponding to different cooling rates increases as the cooling rate decreases, which is the opposite behavior to that in real

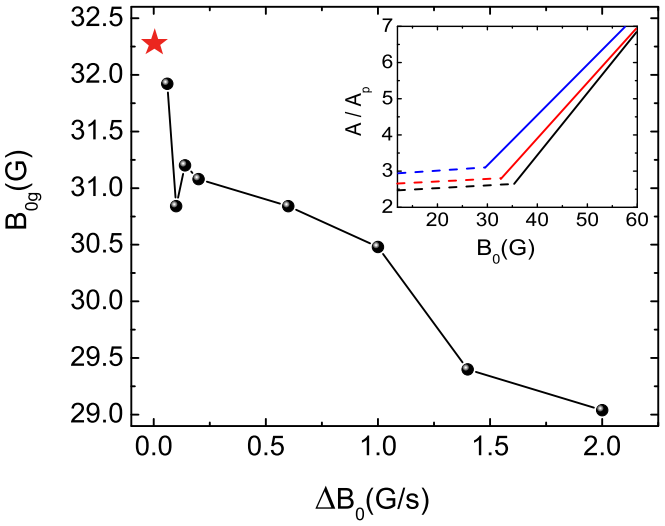

FIG. 6. Glass transition temperature for the amorphous configurations (cooling rates higher than $\Delta B_0 = 0.02$ G/s) in Fig. 5. For $\Delta B_0 = 0.02$ G/s and lower cooling rates the final configurations are crystalline, so we do not define a B_{0g} temperature for those cooling rates. The transition temperature obtained at the threshold cooling rate below which the system always crystallizes is depicted with the red star. Inset: Linear fitting of the evolution of the areas in Fig. 5.

systems. Figure 7 compares the final area occupied by the final configuration as a function of the cooling rate, ΔB_0. In this graph, we observe that the shrinkage of the system is greater when the cooling rate is slower.

IV. VORONOI POLYGONS

We determine some structural characteristics of the system using Voronoi tessellation techniques. For such purpose, polygons are built based on the closest neighbors, giving us

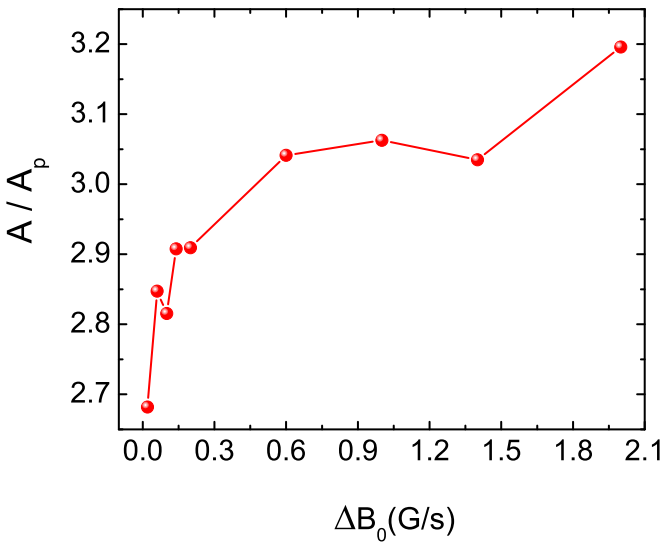

FIG. 7. Final surface occupied by the particles at different cooling steps. This area is normalized with the total area of the particles A_p.

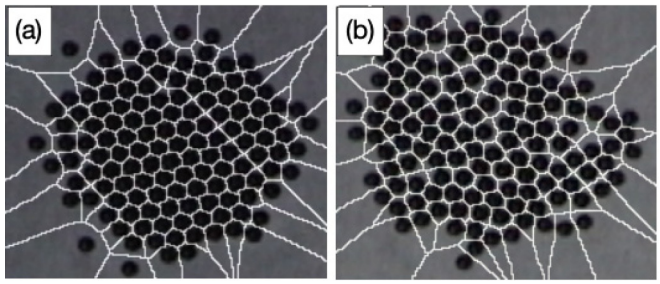

FIG. 8. Comparison between the Voronoi polygons of an ordered (crystal) configuration (a) and a disordered (glass) configuration (b). The polygons at the edges are not taken into account in the analysis.

information about the effective area where the particles move [27]. Numerical studies have also shown that the distribution of the Voronoi areas can be used to discriminate between different phases. Here we study Voronoi polygons obtained from different particle configurations. Using ImageJ we digitally treat the images to obtain binary images and apply a watershed filter to separate the particles from each other. In the watershed segmentation, the Euclidean distance map is first determined and then the ultimate eroded points [30,31]. Then the maxima were found and the Voronoi process was applied to obtain the tessellations.

In Fig. 8 we show a direct comparison of the Voronoi polygons corresponding to a glass and to a crystal configuration. As it can be seen, the shape of the polygons are more homogeneous for the crystal configuration, and they are mostly hexagons. On the other hand, for the glass configuration there are different kind of polygons. It can be observed that the Voronoi polygons corresponding to the particles at the boundaries are the largest, ending at the boundaries of the image. Thus, in the analysis we exclude those polygons.

Figures 9 and 10 show how the distribution of the areas of the polygons evolves in time, for $\Delta B_0 = 2$ G/s and

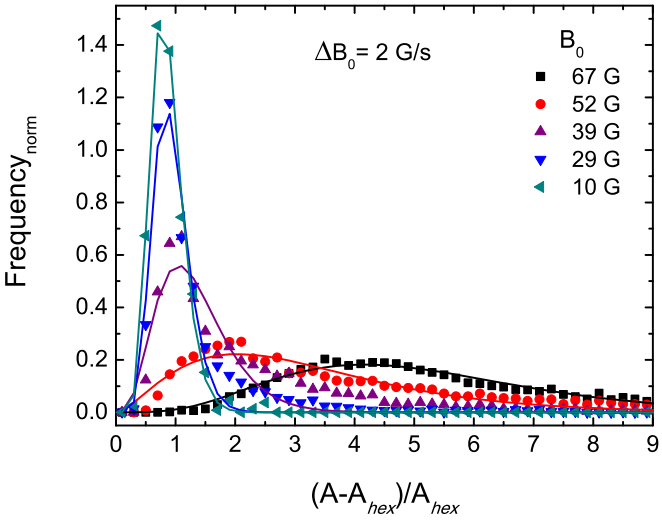

FIG. 9. Distribution of the areas of the Voronoi polygons as we cool the system from a gas phase to a solid phase, with $\Delta B_0 = 2$ G/s. The distributions are fitted to a two-parameter γ distribution (solid lines).

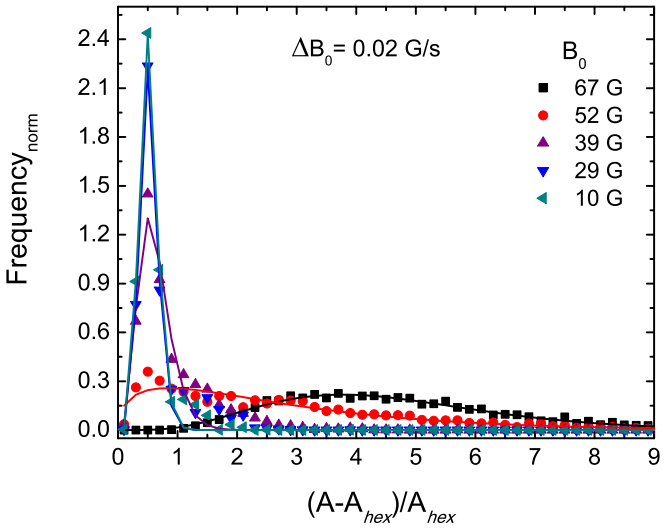

FIG. 10. Distribution of the areas of the Voronoi polygons as the system experiments gas-to-solid phase transition with $\Delta B_0 = 0.02$. The distributions are fitted to a two-parameter γ distribution (solid lines).

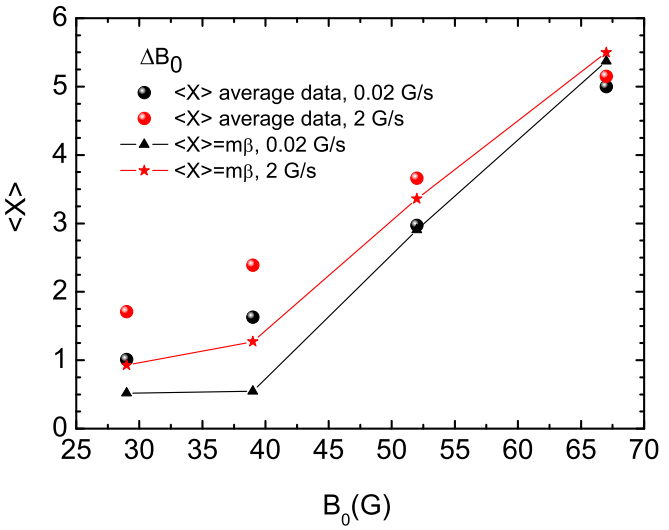

FIG. 11. Expected value of the Voronoi areas for $\Delta B_0 = 0.02$ and $\Delta B_0 = 0.2$ at different temperatures. The expected value $\langle x\rangle = m\beta$ is compared directly with the average value of $x = A - A_{\rm hex})/A_{\rm hex}$ (spheres).

$\Delta B_0 = 0.02$ G/s, respectively. Here we obtain the difference between the Voronoi polygons area (A) and the area of a hexagon circumscribed in the circle drawn by a single bead ($A_{\rm hex}$), normalized with the latter, i.e., $(A - A_{\rm hex})/A_{\rm hex}$. There are two notable characteristics in the distributions. The first one is that at high temperatures the distribution is wide, as the system is in a gas phase. As time passes, the distribution becomes narrower, and at the end, it becomes very sharp. The second characteristic is that the peak of the distribution is shifted to lower values as the system is cooled. At the end, most of the polygons become small, indicating that the structure gets stuck in a solid phase. As one can see in Figs. 9 and 10, the polygons do not reach the minimum value $A_{\rm hex}$, but those with lower cooling rate reach smaller values. The solid lines in these figures are fits of the distributions of the polygons areas to a two-parameter γ distribution,

$$f(x) = [\beta^{-m}/\Gamma(m)]x^{m-1}\exp(-x/\beta), \qquad (1)$$

where m is called the regularity factor and $x = (A - A_{\rm hex})/A_{\rm hex}$. From the fitting, we obtain m and β and so the expected value $\langle x\rangle = m\beta$. This quantity decreases when the area distribution is narrower, i.e., when the configuration is more regular, and is close to zero at a regular close packing.

For a perfect crystal, $\langle x\rangle$ is zero because all of the Voronoi polygons have the same area, which is the minimum area $A_{\rm hex}$. For the glassy state and nonperfect crystals, $\langle x\rangle$ is higher than zero. Temperature increases the kinetic energy of the particles, driving the system to a more disordered configuration and, therefore, to an increase of $\langle x\rangle$. Figure 11 shows the evolution of the expected value $\langle x\rangle$ of the Voronoi areas as a function of the magnetic field for the faster and the slower cooling rates. From the curves, it is clear that the system has a more regular final configuration as the magnetic field decreases. For slow cooling rates, the expected value of the areas is smaller than for faster rates. In Fig. 12 we depict the expected value of the areas for the different cooling rates studied here. This curve depicts the degree of homogeneity of the system; for slow cooling rates this value is smaller because the configuration is more homogeneous than for the fast cooling rates.

In Figs. 11 and 12 the expected value $\langle x\rangle = m\beta$ is compared directly with the average value of $x = (A - A_{\rm hex})/A_{\rm hex}$. From these figures one can observe that even though both values do not coincide qualitatively, the general trend is similar. The reason for this difference is that we have a small number of data, and adjusting to the γ function fails to fully capture the distribution; however, it does capture the trend.

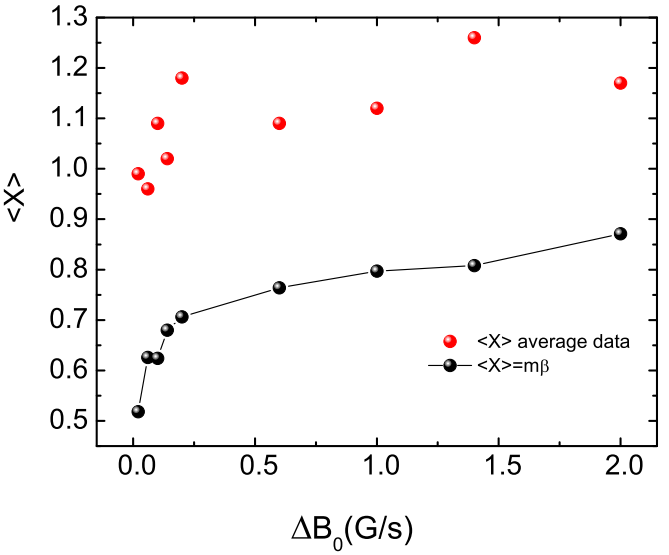

FIG. 12. Expected value of the areas for different cooling steps. The red spheres depict the average value taken directly from the data $x = (A - A_{\rm hex})/A_{\rm hex}$.

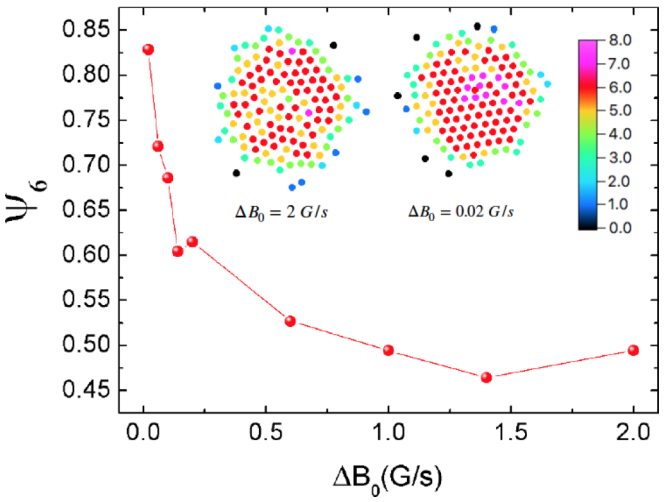

FIG. 13. Average values of the sixfold bond orientational order parameter for the final configurations at different cooling rates. The number of neighbors for each particle is depicted for the fastest and the slowest cooling rate.

The degree of order can also be seen in the sixfold bond orientational order parameter,

$$\psi_6 = \frac{1}{N}\sum_{i=1}^{N}\frac{1}{N_i}\sum_{j}\exp(6i\theta_{ij}), \tag{2}$$

where the sum on j is over the N_i neighbors of this particle and θ_{ij} is the angle between the particles i and j and N is the number particles considered in the calculation, particles at the edge configuration were ignore. Here neighbor particles were determine by using Delaunay triangulations. When $\psi_6 = 1$ the phase is ordered and is disordered as it approaches zero.

From Fig. 13 we can corroborate that, as outlined before, for low cooling rates the final structure is close to a crystalline hexagonal system, while for fast cooling rates we obtain a disordered configuration. In the figure, the color diagram depicts the number of neighbors of each particle.

V. CONCLUSION

We use a macroscopic system to study the process of solidification at several cooling rates. In previous works, we studied such system in the case of spatial homogeneous conditions, and no crystallization was observed. Here we introduce an inhomogeneity in the particles distribution by settling them on a spherical surface which induces an attractive force on the particles toward the bottom of the curved surface. Under such spatial inhomogeneous condition, we observed that different cooling rates produce different final particle structures. For the highest cooling rates, the final configurations are glasslike structures while for the lowest cooling rate studied here the final structure is crystalline. For intermediate cooling rates, it is possible to observe polycrystalline substructures. Thus, in our system, polycrystalline structures precedes crystal structures.

Our system allows us to directly observe the dynamics of the particles at different conditions. Thus, as temperature decreases, particles spend more time in regions close to the center of the lens. The presence of an attraction center in combination with a low kinetic energy makes it possible the formation of a small aggregate at the center, which indicates that the solidification process starts. A particle can fall in a local minimum of energy; however, this condition can be unstable. The constant collisions between neighboring particles can push it away. Then the particle continues moving and eventually it would fall in a deeper minimum of energy and it reminds there. As the temperature continues decreasing, particles finally get arrested in determined positions. As mentioned above, the final structures depend on the cooling rate. Thus, if the cooling rate is very fast, then particles falling in a local minimum of energy, not necessarily the deepest one, remain there. If the cooling rate is very low, then a particle goes from one minimum to another and, finally, the probability of finding a deeper minimum of energy is high and the particle gets arrested in that position. It is observed that sometimes the particle falls in positions that are not the deepest energy ones. However, the random kicking of the surrounding particles push them eventually toward a deeper energy position.

Another interesting feature of the system studied here is that as the cooling rate decreases the glass transition temperature increases in clear contrast with the case of the glass transition in spatially homogeneous samples. In that case, the glass transition temperature decreases as the cooling rate decreases. In our case, as the cooling rate decreases, the behavior of the system changes continuously from glasslike behavior to crystalline structure, passing through the polycrystalline case.

Finally, let us mention that in the system discussed here, one can control the interparticle interactions by applying a constant magnetic field. Also the protocol of the cooling can be easily modified. Additionally, the particle concentration and temperature can be controlled separately, which is a very attractive advantage over others macroscopic systems. Thus, this system provides a simple but versatile model to explore the process of solidification under different conditions.

ACKNOWLEDGMENTS

The partial financial support by CONACyT, México, through Grants No. 80629 and No. 256176 (SEP-Ciencia Básica) and Grant No. 440 (Fronteras de la Ciencia) is acknowledged.

[1] P. G. Debenedetti and F. H. Stillinger, Nature **410**, 259 (2001).
[2] M. D. Ediger, C. A. Angell, and S. R. Nagel, J. Phys. Chem. **100**, 13200 (1996).
[3] G. L. Hunter and E. Weeks, Rep. Prog. Phys. **75**, 066501 (2012).
[4] E. R. Weeks, J. C. Crocker, A. C. Levitt, A. Schofield, and D. A. Weitz, Science **287**, 627 (2000).

[5] P. N. Pusey, Science **332**, 802 (2011).
[6] T. Li, S. Kheifets, D. Medellin, and M. G. Raizen, Science **328**, 1673 (2010).
[7] R. Huang, I. Chavez, K. M. Taute, B. Lukić, S. Jeney, M. G. Raizen, and E. L. Florin, Nat. Phys. **7**, 576 (2011).
[8] H. König, K. Zahn, and G. Maret, in *Slow Dynamics in Complex Systems: 3rd International Symposium on Slow Dynamics in Complex Systems*, edited by M. Tokuyama and I. Oppenheim, AIP Conf. Proc. No. 708 (AIP, New York, 2004).
[9] H. Konig, Europhys. Lett **71**, 838 (2005).
[10] H. König, R. Hund, K. Zahn, and G. Maret, Eur. Phys. J. E **18**, 287 (2005).
[11] L. Assoud, F. Ebert, P. Keim, R. Messina, G. Maret, and H. Löwen, J. Phys.: Condens. Matter **21**, 464114 (2009).
[12] F. Ebert, P. Dillmann, G. Maret, and P. Keim, Rev. Sci. Instrum. **80**, 083902 (2009).
[13] P. M. Reis, R. A. Ingale, and M. D. Shattuck, Phys. Rev. E **75**, 051311 (2007).
[14] R. Cafiero, S. Luding, and H. J. Herrmann, Phys. Rev. Lett. **84**, 6014 (2000).
[15] D. L. Blair and A. Kudrolli, Phys. Rev. E **67**, 021302 (2003).
[16] A. Panaitescu and A. Kudrolli, Phys. Rev. E **81**, 060301(R) (2010).
[17] P. Ramírez-González and M. Medina-Noyola, Phys. Rev. E. **82**, 061504 (2010).
[18] F. Rietz, C. Radin, H. L. Swinney, and M. Schroter, Phys. Rev. Lett. **120**, 055701 (2018).
[19] A. Panaitescu, K. A. Reddy, and A. Kudrolli, Phys. Rev. Lett. **108**, 108001 (2012).
[20] D. A. Morales-Barrera, G. Rodríguez-Gattorno, and O. Carvente, Phys. Rev. Lett. **121**, 074302 (2018).
[21] J.-C. Tsai, G. A. Voth, and J. P. Gollub, Phys. Rev. Lett. **91**, 064301 (2003).
[22] K. E. Daniels and R. P. Behringer, Phys. Rev. Lett. **94**, 168001 (2005).
[23] P. M. Reis, R. A. Ingale, and M. D. Shattuck, Phys. Rev. Lett. **96**, 258001 (2006).
[24] F. Donado, R. E. Moctezuma, L. López-Flores, M. Medina-Noyola, and J. L. Arauz-Lara, Sci. Rep. **7**, 12614 (2017).
[25] C. Tapia-Ignacio, J. Garcia-Serrano, and F. Donado, Phys. Rev. E **94**, 062902 (2016).
[26] F. Donado, J. M. Sausedo-Solorio, and R. E. Moctezuma, Phys. Rev. E **95**, 022601 (2017).
[27] R. E. Moctezuma, J. L. Arauz-Lara, and F. Donado, Physica A **496**, 27 (2018).
[28] M. J. Sánchez-Miranda, J. L. Carrillo-Estrada, and F. Donado, Sci. Rep. **9**, 3531 (2019).
[29] See Supplemental Material at http://link.aps.org/supplemental/10.1103/PhysRevE.101.052907 for Video1, Video2, and Video3 to observe the dynamics at cooling rates 2 G/s, 0.2 G/s, and 0.02 G/s, respectively.
[30] I. F. Sbalzarini and P. Koumoutsakos, J. Struct. Biol. **151**, 182 (2005).
[31] S. A. Schneider, W. S. Rasband, and K. W. Eliceiri, Nat. Methods **9**, 671 (2012).

Correction: An experimental data point depicted as a red star was missing in Figure 6 and has been fixed.